



# <sup>3</sup>He-rich Solar Energetic Particles from Sunspot Jets

Radoslav Bučík<sup>1,2</sup>, Mark E. Wiedenbeck<sup>3</sup>, Glenn M. Mason<sup>4</sup>,  
Raúl Gómez-Herrero<sup>5</sup>, Nariaki V. Nitta<sup>6</sup>, and Linghua Wang<sup>7</sup>

<sup>1</sup>Institut für Astrophysik, Georg-August-Universität Göttingen, D-37077 Göttingen, Germany; [bucik@mps.mpg.de](mailto:bucik@mps.mpg.de)

<sup>2</sup>Max-Planck-Institut für Sonnensystemforschung, D-37077 Göttingen, Germany

<sup>3</sup>Jet Propulsion Laboratory, California Institute of Technology, Pasadena, CA 91109, USA

<sup>4</sup>Applied Physics Laboratory, Johns Hopkins University, Laurel, MD 20723, USA

<sup>5</sup>Space Research Group, University of Alcalá, E-28871 Alcalá de Henares, Spain

<sup>6</sup>Lockheed Martin Advanced Technology Center, Palo Alto, CA 94304, USA

<sup>7</sup>Institute of Space Physics and Applied Technology, Peking University, 100871 Beijing, People's Republic of China

Received 2018 October 18; revised 2018 November 21; accepted 2018 November 22; published 2018 December 12

## Abstract

Solar sources of suprathermal ( $<1$  MeV nucleon<sup>-1</sup>) <sup>3</sup>He-rich solar energetic particles (SEPs) have been commonly associated with jets originating in small, compact active regions at the periphery of near-equatorial coronal holes. Sources of relatively rare, high-energy ( $>10$  MeV nucleon<sup>-1</sup>) <sup>3</sup>He-rich SEPs remain unexplored. Here we present two of the most intense <sup>3</sup>He-rich (<sup>3</sup>He/<sup>4</sup>He  $> 1$ ) SEP events of the current solar cycle 24 measured on the *Advanced Composition Explorer* at energy  $>10$  MeV nucleon<sup>-1</sup>. Although <sup>3</sup>He shows high intensities,  $Z > 2$  ions are below the detection threshold. The events are accompanied by type-III radio bursts, but no type-II emission as typically seen for suprathermal <sup>3</sup>He-rich SEPs. The corresponding solar sources were analyzed using high-resolution, extreme-ultraviolet imaging and photospheric magnetic field observations on the *Solar Dynamics Observatory*. We find the sources of these events associated with jets originating at the boundary of large sunspots with complex  $\beta\gamma\delta$  magnetic configuration. Thus, details of the underlying photospheric field apparently are important to produce <sup>3</sup>He to high energies in the examined events.

**Key words:** acceleration of particles – Sun: abundances – Sun: flares – Sun: magnetic fields – Sun: particle emission

**Supporting material:** animation

## 1. Introduction

<sup>3</sup>He-rich solar energetic particles (SEPs) are characterized by a peculiar ion composition markedly different from the corona or solar wind (e.g., Kocharov & Kocharov 1984; Mason 2007). The abundance of <sup>3</sup>He is enhanced by factors up to 10<sup>4</sup>; heavy (Ne–Fe) and ultra-heavy ions ( $Z > 30$ ) show enhancement by factors  $\sim 3$ –10 and  $>100$ , respectively, independently of <sup>3</sup>He enhancement (Mason et al. 1986, 2004; Reames et al. 1994; Reames & Ng 2004). <sup>3</sup>He-rich SEPs are firmly associated with type-III radio bursts (e.g., Nitta et al. 2006) and their parent low-energy electrons (e.g., Wang et al. 2012). A distinct composition of <sup>3</sup>He-rich SEPs is believed to indicate a unique acceleration mechanism operating in their solar sources. A variety of models have been proposed for ion acceleration in <sup>3</sup>He-rich SEP events (see review by Miller 1998). Most models involve ion-cyclotron resonance with plasma waves.

Solar sources of <sup>3</sup>He-rich SEPs have been associated with coronal jets (e.g., Kahler et al. 2001; Nitta et al. 2006, 2008, 2015; Wang et al. 2006b; Bučík et al. 2014, 2018; Chen et al. 2015), indicating acceleration in magnetic reconnection on field lines open to interplanetary (IP) space (e.g., Shimojo & Shibata 2000). The events with high <sup>3</sup>He and heavy-ion enrichments have shown unwinding motions in jets (Innes et al. 2016; Mason et al. 2016; Bučík et al. 2018). In some events, jets were accompanied by large-scale propagating coronal fronts (Nitta et al. 2015; Bučík et al. 2016). Jets in <sup>3</sup>He-rich SEP events have been found to originate at the compact, small active regions near the coronal holes (Pick et al. 2006; Wang et al. 2006b; Bučík et al. 2018). There are reports on <sup>3</sup>He-rich jets from a plage region (Chen et al. 2015) or

sunspot umbra (Nitta et al. 2008). All of these studies are based on ion measurements below a few MeV nucleon<sup>-1</sup>. Solar sources of relatively rare, high-energy ( $>10$  MeV nucleon<sup>-1</sup>) <sup>3</sup>He-rich SEP events remain unexplored although these events were for the first time detected at 10–100 MeV nucleon<sup>-1</sup> (Hsieh & Simpson 1970).

In this Letter, we examine the solar sources of the two most intense high-energy ( $>10$  MeV nucleon<sup>-1</sup>) <sup>3</sup>He-rich SEP events of the present solar cycle 24 (2008–2017). We report that the solar sources of these events are associated with jets originating at the boundary of large sunspots with complex magnetic configurations.

## 2. Methods

On 2011 February 18 and 2015 August 24, two <sup>3</sup>He-rich SEP events were identified using measurements from the Solar Isotope Spectrometer (SIS; Stone et al. 1998) on the *Advanced Composition Explorer* (ACE). The SIS is a  $dE/dx$  versus residual energy telescope, measuring He to Zn nuclei from  $\sim 4$  to  $\sim 100$  MeV nucleon<sup>-1</sup>. The reported events show the highest <sup>3</sup>He intensities among all of the other highly enriched (<sup>3</sup>He/<sup>4</sup>He  $> 1$ ) SEP events at energy 10.5 MeV nucleon<sup>-1</sup> in the examined 10 year period. Note that in the solar wind <sup>3</sup>He/<sup>4</sup>He  $\sim 4 \times 10^{-4}$  (e.g., Gloeckler & Geiss 1998). The Electron Proton Helium Instrument (EPHIN; Müller-Mellin et al. 1995) measurements aboard *SOHO* confirm that these two events show the highest <sup>3</sup>He intensities in the energy range 5–25 MeV nucleon<sup>-1</sup>. The EPHIN has a similar measurement principle as SIS but a smaller geometric factor. Low-energy abundances were examined using the Ultra Low Energy

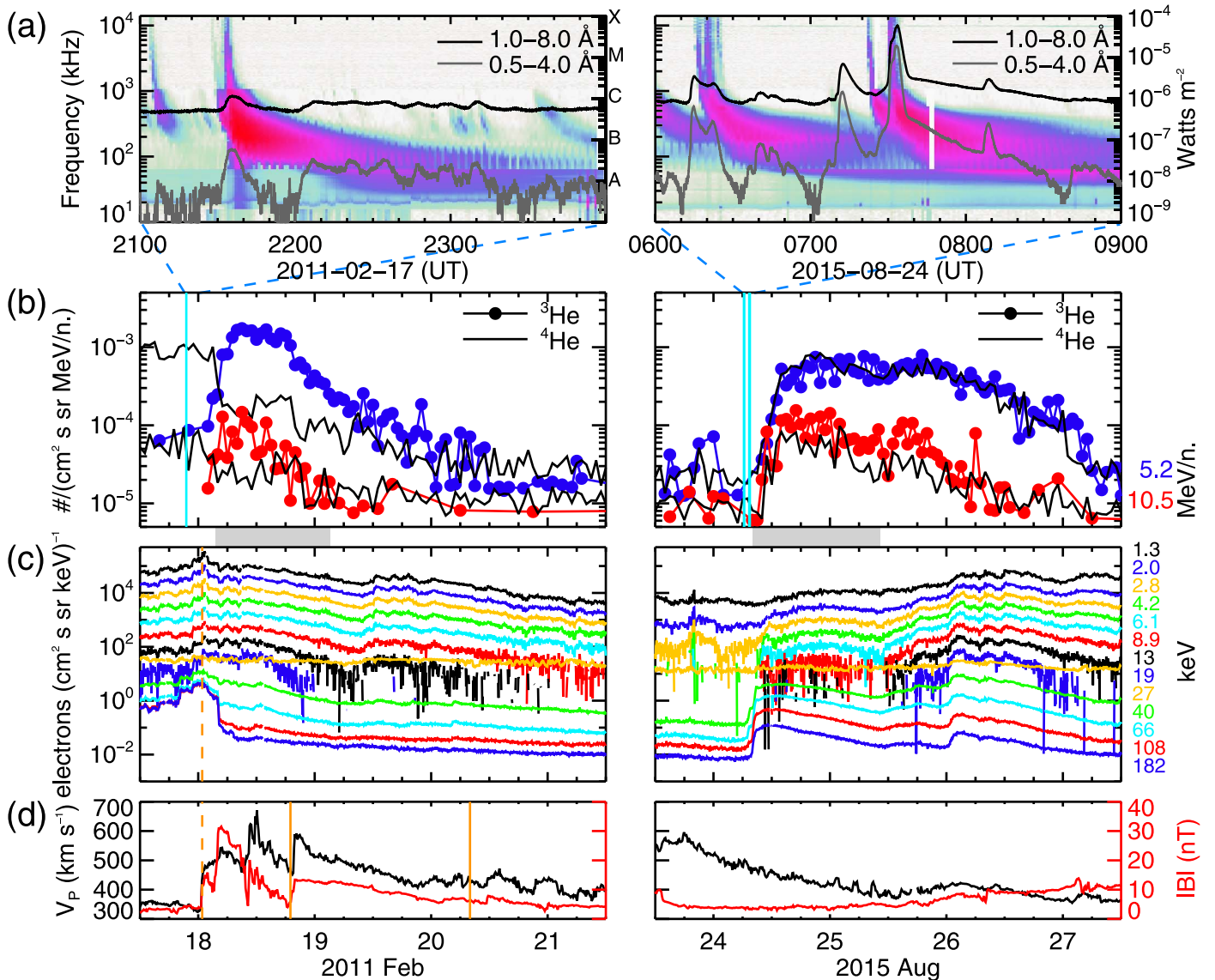


**Figure 1.** (a) 1 minute *Wind*/WAVES radio spectrogram and GOES-15 2 s X-ray fluxes (two curves). The labels A, B, C, M, and X indicate flare classes in the 1–8 Å channel. (b) 1 hr *ACE*/SIS 5.2 and 10.5 MeV nucleon $^{-1}$   $^3He$ ,  $^4He$  intensities. The upper (lower) curve shows the lower (higher)-energy  $^4He$  intensities. Solid vertical lines mark the event-associated type-III bursts shown in panel (a). Gray shaded bars mark the periods considered for analysis in each event. (c) 5 minutes electron intensities from *Wind*/3DP (1.3–182 keV). The dashed vertical line marks the IP shock. (d) 10 minutes solar wind speed  $V_p$  (black) and magnetic field magnitude  $|B|$  (red). Solid vertical lines mark the ICME time interval.

Isotope Spectrometer (ULEIS; Mason et al. 1998) on *ACE*. The ULEIS is a time-of-flight mass spectrometer that measures ions in the energy range from 20 keV nucleon $^{-1}$  to several MeV nucleon $^{-1}$ . We also make use of energetic electron measurements made by the 3DP EESA-H and *semiconductor detector telescopes* (SST; Lin et al. 1995) on *Wind*, solar wind measurements made by the Solar Wind Electron Proton Alpha Monitor (SWEPAM; McComas et al. 1998) and Magnetometer (MAG; Smith et al. 1998) on *ACE*. *ACE*, *SOHO*, and *Wind* were in the IP space at the L1 point.

The solar sources of  $^3He$ -rich SEPs were investigated using high-resolution observations from the Atmospheric Imaging Assembly (AIA; Lemen et al. 2012) and Helioseismic and Magnetic Imager (HMI; Scherrer et al. 2012) on the *Solar Dynamics Observatory* (*SDO*). The AIA provides full-disk images of the Sun with  $1''/5$  spatial and 12 s temporal resolution at seven extreme-ultraviolet (EUV) and three ultraviolet (UV)

wavelength channels. We use 304, 171, and 193 Å channels that observe emissions from He II ( $\sim 0.08$  MK), Fe IX ( $\sim 0.8$  MK) and Fe XII ( $\sim 1.5$  MK) lines, respectively. The HMI provides full-disk line-of-sight magnetograms and continuum intensity images with a spatial resolution of  $1''$  and a cadence of 45 s. We also inspect *Wind* WAVES (Bougeret et al. 1995) radio spectra for the event-associated type-III burst. The frequency range of WAVES ( $< 14$  MHz) covers emissions generated from about two solar radii to 1 au. Furthermore, we make use of soft X-ray observations from the NOAA GOES-15 XRS sensor.

### 3. Results

#### 3.1. $^3He$ -rich SEP Events

Figure 1 shows the energetic particle and solar wind plasma measurements for two examined  $^3He$ -rich SEP events and the

**Table 1**  
 $^3\text{He}$ -rich SEP Event Properties

SEP Start	Days <sup>a</sup>	$^3\text{He}/^4\text{He}^a$	$^3\text{He}$ Flux <sup>a</sup> ( $\times 10^{-5}$ )	$^3\text{He}/^4\text{He}^b$	Fe/O <sup>b</sup>	Type-III <sup>c</sup> Start	Flare <sup>d</sup>			CME <sup>e</sup>		
							Class	Start	Loc.	Speed	Width	
2011 Feb 18	049.17–050.13	$2.33^{+0.22}_{-0.17}$	$5.26^{+0.49}_{-0.38}$	$0.12 \pm 0.01$	$1.46 \pm 0.13$	Feb 17 21:32	C1.1	21:30	S19W46	490	82	
2015 Aug 24	236.33–237.42	$1.61^{+0.09}_{-0.07}$	$5.78^{+0.33}_{-0.27}$	$0.24 \pm 0.11$	$1.16 \pm 0.74$	Aug 24 06:16	...	...	S14E01	...	...	
							Aug 24 06:20	C2.3	06:20	"	...	...
							Aug 24 07:22	C1.3	07:22	S14W00	...	...
							Aug 24 07:30	M5.6	07:26	"	272	88

**Notes.**

<sup>a</sup> 10.5 MeV nucleon<sup>-1</sup>; flux units—particles (cm<sup>2</sup> s sr MeV nucleon<sup>-1</sup>)<sup>-1</sup>.

<sup>b</sup> 0.546 MeV nucleon<sup>-1</sup>.

<sup>c</sup> ~10 MHz from *Wind*/WAVES 1 minute data.

<sup>d</sup> GOES X-ray class and start; location in *SDO*/AIA 304 Å.

<sup>e</sup> Coronal Mass Ejection (CME) speed (km s<sup>-1</sup>), width (°) from *SOHO*/LASCO catalog ([http://cdaw.gsfc.nasa.gov/CME\\_list](http://cdaw.gsfc.nasa.gov/CME_list)).

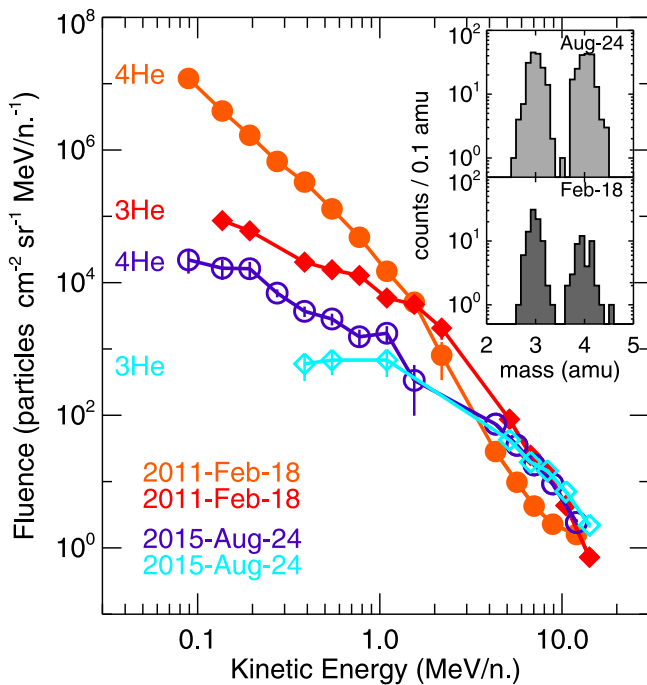


**Figure 2.** Energy spectra of  $^4\text{He}$  (circles) and  $^3\text{He}$  (diamonds) for the 2011 February 18 (solid) and 2015 August 24 (open symbols) events measured with ULEIS (eight  $^3\text{He}$  and ten  $^4\text{He}$  energy bins; see the text for an explanation of the missing spectral points) and SIS (five energy bins). Inset:  $^3\text{He}$  ( $^4\text{He}$ ) mass histograms at 10.5 (8.9) MeV nucleon<sup>-1</sup>. The SIS energy intervals correspond to intervals of ranges of ions (depths in the detector stack), resulting in a slightly lower energy per nucleon for  $^4\text{He}$  than for  $^3\text{He}$ .

associated radio and soft X-ray activity. Figure 1(a) displays *Wind*/WAVES radio spectrograms and the GOES X-ray fluxes. Figure 1(b) shows 1 hr *ACE*/SIS  $^3\text{He}$ ,  $^4\text{He}$  intensities at 5.2 and 10.5 MeV nucleon<sup>-1</sup>.  $^4\text{He}$  intensities below  $\sim 10^{-5}$  should be regarded as upper limits. Figure 1(c) presents *Wind*/3DP electron intensities at different energy channels (EESA-H 1.3–19 keV and SST 27–182 keV). Figure 1(d) shows the solar wind speed and magnetic field magnitude.

The 2011 February 18 event occurred during the decay phase of the gradual SEP event of 2011 February 15 and near the passage of an IP fast forward shock on 2011 February 18 00:49 UT. Figure 1 indicates that after the shock passage the  $^3\text{He}$  intensity starts to increase, while  $^4\text{He}$  intensity decreases. The

opposite time-intensity profiles suggest that the event onset near the shock passage was most likely coincidental. The shock on *Wind* has been reported at Harvard-Smithsonian Center for Astrophysics IP Shock Database (<https://www.cfa.harvard.edu/shocks/>). The corresponding IP coronal mass ejection (ICME) can be found in the list of the Near-Earth ICMEs (<http://www.srl.caltech.edu/ACE/ASC/DATA/level3/icmetable2.html>). To confirm the solar origin of the 2011 February 18 event we examined the ULEIS/SIS He mass spectrograms of individual ions in the energy ranges 0.4–1.0 and 7.6–16.3 MeV nucleon<sup>-1</sup>, available at the ACE science center (<http://www.srl.caltech.edu/ACE/ASC/DATA/level3/sis/heplots>). The spectrograms indicate the velocity dispersive onset for the 2011 February 18 event. In 0.4–1.0 and 7.6–16.3 MeV nucleon<sup>-1</sup> energy ranges the first  $^3\text{He}$  ions appeared at ~05–06 UT and ~02–03 UT, respectively. The time lag between the onsets (3 hr) is consistent with the propagation time difference (257–63 minutes) for ions in these two energy intervals traveling from Sun to L1 along the nominal Parker field line. The 2011 February 18 event is included in a statistical study of Fe-rich SEP events in 1995–2013 (Reames et al. 2014) with Fe/O =  $1.34 \pm 0.20$  (at 3–4 MeV nucleon<sup>-1</sup>). Note that the intensity of  $Z > 2$  ions, including Fe, at energy  $> 10$  MeV nucleon<sup>-1</sup> on SIS was below the measurable level for both events. The ULEIS confirms that at low energies both events are Fe-rich with Fe/O  $\sim 1$  (see Table 1). Soft energy spectra and low  $Z > 2$  abundances (relative to He) in  $^3\text{He}$ -rich events frequently preclude SIS detection of these elements.

Solar energetic electrons were not clearly measured in the 2011 February 18 event due to enhanced background related to the preceding gradual SEP event and the passage of the IP shock. Furthermore, the electron channels at  $\geq 108$  keV were contaminated by protons. Note that the SST data were corrected for scattered electrons that leave only a fraction of their energy in the detector (Wang et al. 2006a). An association with type-III radio bursts is rather straightforward as there were no other significant type-III bursts in the 11 hr interval before the event start time. The event-associated type-III burst on February 17 21:32 UT was accompanied by a C3.1 X-ray flare (see Figure 1(a), left panel). The associations are consistent with the analysis by Reames et al. (2014). The 2015 August 24 event was accompanied by two consecutive solar energetic electron events, separated by  $\sim 1$  hr. For this reason, the first electron intensity enhancement, notably weaker (measured at

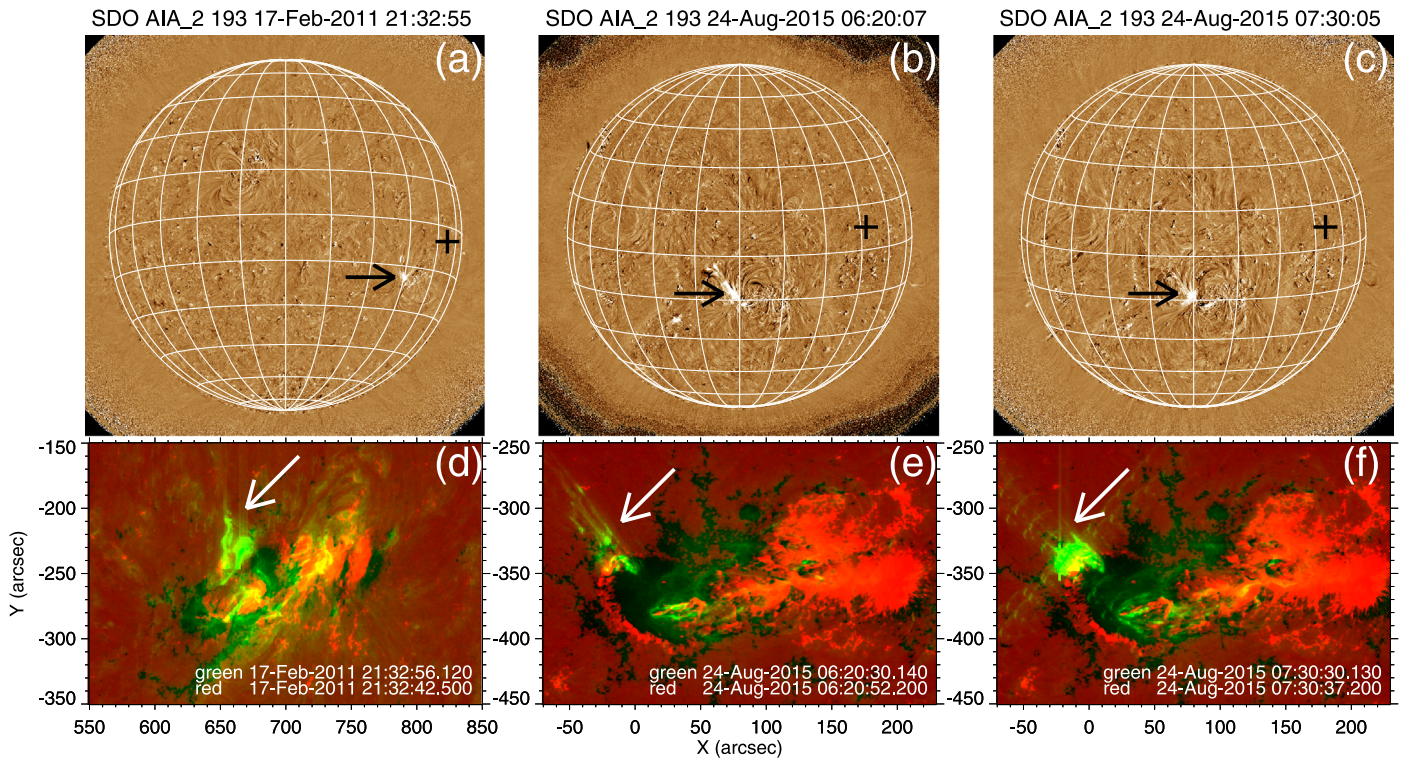


**Figure 3.** (a)–(c) *SDO* AIA 193 Å 1 minute base-difference images at start time of the type-III bursts for the 2011 February 18 (panel (a)) and 2015 August 24 (panels (b) and (c)) events. Pluses mark the L1 magnetic foot-point. The arrows point to the source flares/jets. The heliographic longitude–latitude grid has  $15^\circ$  spacing. (d)–(f) Two-color composite images at start time of the type-III bursts for the 2011 February 18 (panel (d)) and 2015 August 24 (panels (e) and (f)) events. The AIA 304 Å images correspond to green and the HMI line-of-sight magnetic field (scaled to  $\pm 200$  G) to red/black.

(An animation of this figure is available.)

$<100$  keV) than the second, is not well resolved. Each electron event is associated with a double type-III burst; in the first electron event, the type-III bursts are separated by 4 minutes and in the second event by 8 minutes. The type-III bursts on August 24 06:16 and 06:20 UT, related to the first electron event, occurred near a double X-ray flux enhancement (see Figure 1(a), right panel) corresponding to the C3.2 and C2.3 flares. The high-cadence EUV images suggest that the type-III burst at 06:16 UT is likely unrelated to the C3.2 flare (see Section 3.2). The type-III bursts on August 24 7:22 and 7:30 UT, related to the second electron event, were accompanied by C1.3 and M5.6 flares, respectively. The C1.3 flare, not well resolved from elevated X-ray flux during the decay phase of previous stronger flare, was identified with the help of 0.5–4 Å GOES channel. None of the examined events have type-II bursts arising from coronal shocks. The events were accompanied by only slow coronal mass ejections (CMEs; see Table 1).

Figure 2 shows  $^4\text{He}$ ,  $^3\text{He}$  ULEIS, and SIS fluence spectra for the two examined events. The He mass histograms integrated over the duration of the events are embedded in Figure 2. The  $^4\text{He}$  fluence in the February 18 event should be treated as upper limit due to the possibility of a contribution from the preceding event. Note that the  $^3\text{He}$  intensity increase on August 25 (see Figure 1(b), right panel), probably associated with the same active region as the August 24 event, is not included in the calculation of the event characteristics. Missing ULEIS spectral points (five for  $^3\text{He}$  and one for  $^4\text{He}$ ) for the August 24 event means that the fluence was near the lowest measurable level (zero or one count in the integrated period). It is surprising that below  $\sim 1$  MeV nucleon $^{-1}$  the 2015 August 24 event is at the

threshold level, though at  $>10$  MeV nucleon $^{-1}$  it is one of the most intense  $^3\text{He}$ -rich events in the solar cycle. The energy spectra are roughly consistent with double power laws where slopes are harder below  $\sim 1.5$  MeV nucleon $^{-1}$ .

Table 1 summarizes the characteristics of the examined events. Column 1 gives the particle event start date, and column 2 shows the  $^3\text{He}$ -rich period where fluences/abundances were determined. Columns 3 and 4 indicate the average  $^3\text{He}/^4\text{He}$  ratio and the average  $^3\text{He}$  flux at 10.5 MeV nucleon $^{-1}$ , respectively. Note the enormous 1 hr  $^3\text{He}/^4\text{He}$  ratios in the early stage of the 2011 February 18 event, exceeding a value of 10 at 5.2 MeV nucleon $^{-1}$  (see Figure 1(b), left panel). Columns 5 and 6 give the  $^3\text{He}/^4\text{He}$  and Fe/O ratio at 0.546 MeV nucleon $^{-1}$ , respectively. Column 7 gives the type-III burst start time as observed by *Wind*/*WAVES*. Columns 8 and 9 indicate the GOES X-ray flare class and start time, respectively. Column 10 shows the flare location as observed in *SDO*/AIA 304 Å channel. Columns 11 and 12 give the CME speed and width, respectively, obtained from the *SOHO* LASCOCAT catalog.

### 3.2. Solar Sources

To localize the solar source of the  $^3\text{He}$ -rich SEP events, we have examined high-cadence, full-disk *SDO* AIA images for flaring around the time of the event-associated type-III bursts. Figures 3(a)–(c) show the base-difference images at 193 Å, revealing jets at the type-III burst times. Associated animations show the progress of flaring activity for several minutes around the type-III bursts. Note the relatively large longitudinal ( $\sim 45^\circ$ ) separation between the L1 magnetic foot-point and the associated jets in the August 24 event. The foot-point

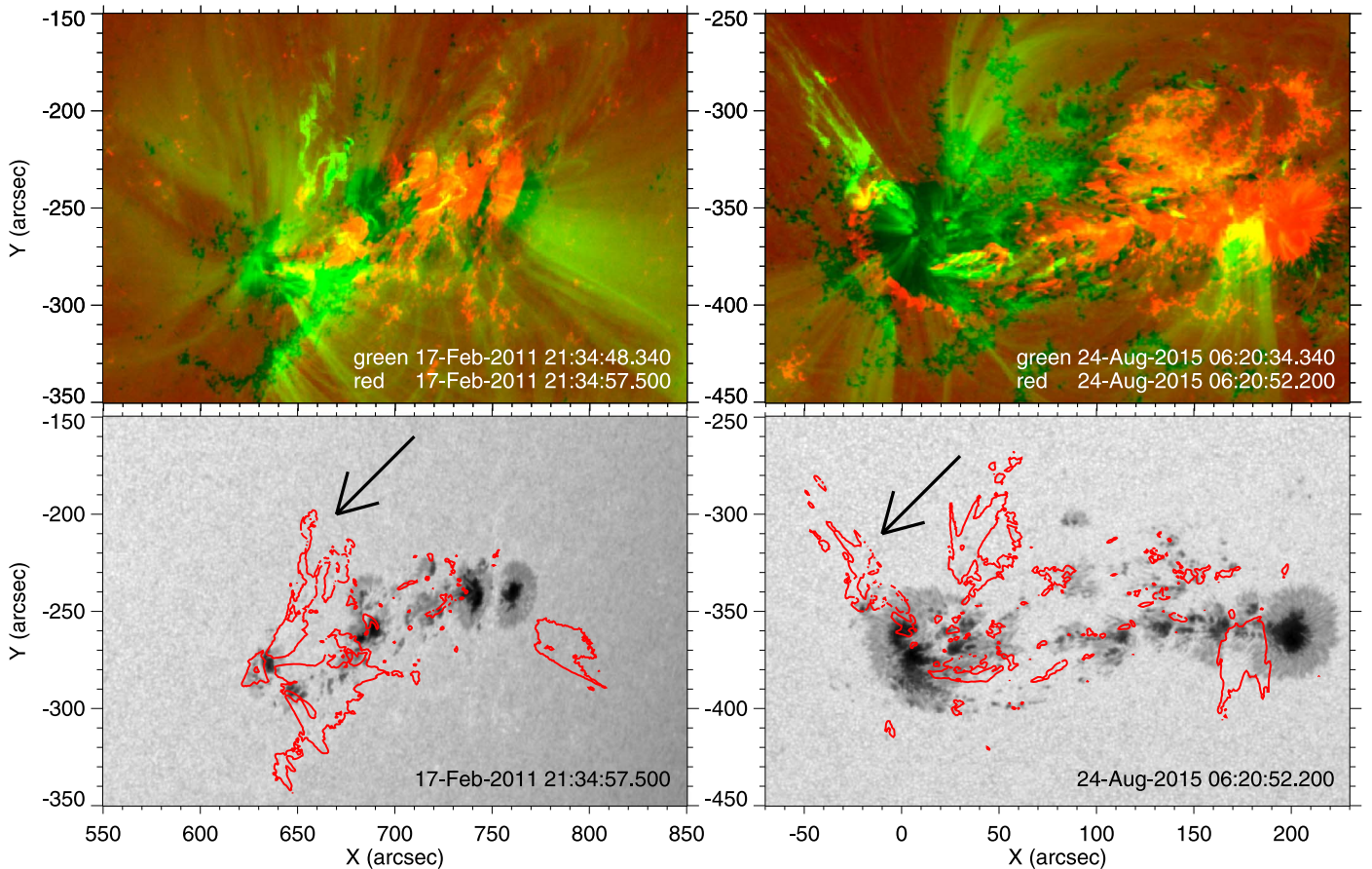


**Figure 4.** Top: same as Figures 3(d), (e) but here the 171 Å image corresponds to green. Bottom: the HMI continuum intensity. Over-plotted contours mark the 95th percentile of intensity in the corresponding 171 Å images. The arrows point to the event-associated jets. The images are for the 2011 February 18 (left) and 2015 August 24 (right) events.

longitude of the Parker spiral connecting L1 was determined from the measured solar wind speed at the type-III burst onset time. In the February 18 event the jet was accompanied by a faint larger-scale front propagating northward; in the August 24 event the jets evolved to a wider eruption.

In order to provide a more detailed view on the event-associated jets and the underlying photospheric magnetic field, Figures 3(d)–(f) show two-color composite images where the AIA 304 Å channel corresponds to green and the HMI line-of-sight magnetic field to red (+black). The black and light-red areas indicate regions with strong magnetic fields of negative and positive polarity, respectively. The images are shown at times of the event-associated type-III bursts (see the animation for other times). In both events, the EUV jets are rooted at the boundary of a large sunspot at the interface with the minor (positive) polarity field. In the February event, the magnetic fields of opposite polarities were separated by about 15''; in the August event, the fields were closely adjacent. The jet in the February event shows a complex helical structure with unwinding counterclockwise motion. The jets in the August event show a structured spire with no obvious rotation. The jet at the onset of the M5.6 flare in the August 24 event was less clearly visible. The animation shows that type-III burst on August 24 06:16 UT coincides with the jet at the sunspot boundary and not with C3.2 flare at 06:13 UT (the first X-ray flux increase in Figure 1(a), right panel) that occurred in the more central part of the sunspot along the closed loops.

Figure 4 (top panels) shows another two-color composite image combining the AIA 171 Å channel and the HMI line-of-sight magnetic field. Here coronal loops, connecting the fields of opposite polarities, and peripheral fan structures are clearly seen. Strikingly, the jets are not co-located with these large-scale coronal structures, which were visible in the sunspots before the events. The jet in the August event appears more complex in 171 Å, but a rotation (as in the February event) is not observed. Figure 4 (bottom) shows the corresponding HMI continuum with over-plotted contours of high (95th percentile) level of intensity from the 171 Å image. The jets in both events appear to be rooted near the sunspot penumbra.

Active region (AR) 11158, associated with the 2011 February 18 event, emerged in the eastern solar hemisphere on February 11. According to the Solar Event List (<ftp://ftp.swpc.noaa.gov/pub/warehouse>), AR 11158 produced 1 B-, 56 C-, 5 M-, and 1 X-class flare during its disk transit. AR 11158 consisted of two major emerging bipoles that showed complex sunspot motion and interaction (e.g., Jiang et al. 2012). AR 12403, associated with the 2015 August 24 event, also contains two major bipoles. AR 12403 appeared near the eastern limb on August 17. During its disk transit, AR 12403 produced 34 B-, 84 C-, 11 M-class flares. Both ARs show a less common  $\beta\gamma\delta$  magnetic classification.<sup>8</sup> The  $\beta\gamma\delta$  class has been reported in  $\sim 4\%$  of all ARs in 1992–2015 (Jaeggli

<sup>8</sup>  $\beta\gamma$  denotes a bipolar sunspot group with no clearly marked line separating spots of opposite polarity;  $\delta$  indicates a penumbra enclosing umbrae of opposite polarity.

& Norton 2016). According to USAF/NOAA Sunspot Group Reports ([https://www.ngdc.noaa.gov/stp/space-weather/solar-data/solar-features/sunspot-regions/usaf\\_mw1/](https://www.ngdc.noaa.gov/stp/space-weather/solar-data/solar-features/sunspot-regions/usaf_mw1/)), AR 12403 was among the 10 largest ARs in the present solar cycle. The maximum reported area was 1320 millionths of the solar hemisphere. The maximum area of AR 11158 was 670.

#### 4. Discussion and Summary




We have examined the solar sources of the two most intense high-energy ( $>10$  MeV nucleon $^{-1}$ )  $^3\text{He}$ -rich SEP events of the current solar cycle. We have found that the solar sources of the  $^3\text{He}$ -rich SEPs were structured jets—in one case with an untwisting motion. A striking feature of the investigated events is their association with jets originating at the boundaries of large and complex sunspots with  $\beta\gamma\delta$  magnetic class. The sunspots produced numerous (63 and 129) X-ray flares during their disk transit. The August 24 event was accompanied by four type-III bursts within one hour, suggesting that the extreme  $^3\text{He}$  intensity may be related to unresolved multiple ion injections. The February 18 event was associated with only a single type-III burst.

Solar sources of high-energy ( $>10$  MeV nucleon $^{-1}$ )  $^3\text{He}$ -rich SEPs have not been specifically tackled in previous studies. Nitta et al. (2015) have reported that about one half (13 out of 29) of their events have energetic  $^3\text{He}$  measured at  $>4.9$  MeV nucleon $^{-1}$ , where 11 events were associated with jets or ejections and 2 with coronal waves. One of those events was associated with a helical jet from an AR near a coronal hole (Innes et al. 2016). Four events in Nitta et al. (2015) that do not show  $^3\text{He}$  at SIS high energies were associated with jets from a plage region (Chen et al. 2015). Bučík et al. (2016) have found that one quarter (8 out of 32) of the events in their survey have  $^3\text{He}$  measured at  $>7.6$  MeV nucleon $^{-1}$ , where 6 events were associated with coronal waves (where a few started as a jet) and 2 with brightening. No information on the photospheric field has been reported for these events. The only  $^3\text{He}$ -rich SEP event associated with sunspot umbral jet did not show an extension of  $^3\text{He}$  measurements to the SIS energy range (Nitta et al. 2008).

Earlier works (Kocharov & Torsti 2003; Torsti et al. 2003) have suggested that high energies of  $^3\text{He}$ -rich SEPs may be due to re-acceleration in coronal shocks. This is unlikely in the events reported here that were accompanied by faint CMEs without a coronal shock signature. An enhancement of suprathermal  $^3\text{He}$  in IP shock events has been reported in Desai et al. (2001). It has been suggested that the  $^3\text{He}$  enhancement is due to an acceleration of remnants from prior  $^3\text{He}$ -rich SEP events (Desai et al. 2001) or a solar particle event is swept up by the shock (Tsurutani et al. 2002). Different time-intensity profiles for  $^3\text{He}$  and  $^4\text{He}$  and a velocity dispersive onset in the February 18 event indicate that the IP shock preceding the event might only marginally affect the  $^3\text{He}$  enhancement. An association with jets from the edge of sunspots with complex magnetic configuration may be a distinct feature of high-energy  $^3\text{He}$ -rich SEP events. It has been known that a large sunspot area and complex magnetic configuration are important to produce the largest flares (e.g., Sammis et al. 2000). We plan to address such relation for production of high-energy  $^3\text{He}$ -rich SEPs in the forthcoming statistical study.

The work of R.B. was supported by DFG grant BU 3115/2-1. The work of M.E.W. was supported under NASA Goddard grant 80NSSC18K0223 to Caltech. Work at JHU/APL was supported by NASA grant NNX17AC05G/125225. R.G.H. acknowledges the financial support of the Spanish MINECO projects ESP2017-88436-R and EPS2015-68266-R. The work by N.V.N. was supported by NSF grant AGS-1259549 and NASA grant 80NSSC18K1126. R.B. and R.G.H. acknowledge the support of the University of Alcalá through the Giner de los Ríos visitor program. We wish to acknowledge Davina Innes for useful discussions and comments.

#### ORCID iDs

Radoslav Bučík  <https://orcid.org/0000-0001-7381-6949>  
 Glenn M. Mason  <https://orcid.org/0000-0003-2169-9618>  
 Raúl Gómez-Herrero  <https://orcid.org/0000-0002-5705-9236>  
 Linghua Wang  <https://orcid.org/0000-0001-7309-4325>

#### References

- Bougeret, J.-L., Kaiser, M. L., Kellogg, P. J., et al. 1995, *SSRv*, 71, 231  
 Bučík, R., Innes, D. E., Mall, U., et al. 2014, *ApJ*, 786, 71  
 Bučík, R., Innes, D. E., Mason, G. M., et al. 2018, *ApJ*, 852, 76  
 Bučík, R., Innes, D. E., Mason, G. M., & Wiedenbeck, M. E. 2016, *ApJ*, 833, 63  
 Chen, N.-H., Bučík, R., Innes, D. E., & Mason, G. M. 2015, *A&A*, 580, A16  
 Desai, M. I., Mason, G. M., Dwyer, J. R., et al. 2001, *ApJL*, 553, L89  
 Gloeckler, G., & Geiss, H. 1998, *SSRv*, 84, 275  
 Hsieh, K. C., & Simpson, J. A. 1970, *ApJL*, 162, L191  
 Innes, D. E., Bučík, R., Guo, L.-J., & Nitta, N. 2016, *AN*, 337, 1024  
 Jaeggli, S. A., & Norton, A. A. 2016, *ApJL*, 820, L11  
 Jiang, Y., Zheng, R., Yang, J., et al. 2012, *ApJ*, 744, 50  
 Kahler, S. W., Reames, D. V., & Sheeley, N. R., Jr. 2001, *ApJ*, 562, 558  
 Kocharov, L., & Torsti, J. 2003, *ApJ*, 586, 1430  
 Kocharov, L. G., & Kocharov, G. E. 1984, *SSRv*, 38, 89  
 Lemen, J. R., Title, A. M., Akin, D. J., et al. 2012, *SoPh*, 275, 17  
 Lin, R. P., Anderson, K. A., Ashford, S., et al. 1995, *SSRv*, 71, 125  
 Mason, G. M. 2007, *SSRv*, 130, 231  
 Mason, G. M., Gold, R. E., Krimigis, S. M., et al. 1998, *SSRv*, 86, 409  
 Mason, G. M., Mazur, J. E., Dwyer, J. R., et al. 2004, *ApJ*, 606, 555  
 Mason, G. M., Nitta, N. V., Wiedenbeck, M. E., & Innes, D. E. 2016, *ApJ*, 823, 138  
 Mason, G. M., Reames, D. V., Klecker, B., Hovestadt, D., & von Rosenvinge, T. T. 1986, *ApJ*, 303, 849  
 McComas, D. J., Bame, S. J., Barker, P., et al. 1998, *SSRv*, 86, 563  
 Miller, J. A. 1998, *SSRv*, 86, 79  
 Müller-Mellin, R., Kunow, H., Fleissner, V., et al. 1995, *SoPh*, 162, 483  
 Nitta, N. V., Mason, G. M., Wang, L., Cohen, C. M. S., & Wiedenbeck, M. E. 2015, *ApJ*, 806, 235  
 Nitta, N. V., Mason, G. M., Wiedenbeck, M. E., et al. 2008, *ApJL*, 675, L125  
 Nitta, N. V., Reames, D. V., DeRosa, M. L., et al. 2006, *ApJ*, 650, 438  
 Pick, M., Mason, G. M., Wang, Y.-M., Tan, C., & Wang, L. 2006, *ApJ*, 648, 1247  
 Reames, D. V., Cliver, E. W., & Kahler, S. W. 2014, *SoPh*, 289, 3817  
 Reames, D. V., Meyer, J. P., & von Rosenvinge, T. T. 1994, *ApJS*, 90, 649  
 Reames, D. V., & Ng, C. K. 2004, *ApJ*, 610, 510  
 Sammis, I., Tang, F., & Zirin, H. 2000, *ApJ*, 540, 583  
 Scherer, P. H., Schou, J., Bush, R. I., et al. 2012, *SoPh*, 275, 207  
 Shimojo, M., & Shibata, K. 2000, *ApJ*, 542, 1100  
 Smith, C. W., L'Heureux, J., Ness, N. F., et al. 1998, *SSRv*, 86, 613  
 Stone, E. C., Cohen, C. M. S., Cook, W. R., et al. 1998, *SSRv*, 86, 357  
 Torsti, J., Kocharov, L., Laivola, J., Chertok, I., & Thompson, B. J. 2003, *SoPh*, 214, 177  
 Tsurutani, B. T., Zhang, L. D., Mason, G. M., et al. 2002, *AnGeo*, 20, 427  
 Wang, L., Lin, R. P., Krucker, S., & Gosling, J. T. 2006a, *GeoRL*, 33, L03106  
 Wang, L., Lin, R. P., Krucker, S., & Mason, G. M. 2012, *ApJ*, 759, 69  
 Wang, Y.-M., Pick, M., & Mason, G. M. 2006b, *ApJ*, 639, 495